

A Mathematical Study of the Influence of Hypoxia and Acidity on the Evolutionary Dynamics of Cancer

Original

A Mathematical Study of the Influence of Hypoxia and Acidity on the Evolutionary Dynamics of Cancer / Fiandaca, G.; Delitala, M.; Lorenzi, T.. - In: BULLETIN OF MATHEMATICAL BIOLOGY. - ISSN 0092-8240. - 83:7(2021), p. 83. [10.1007/s11538-021-00914-3]

Availability:

This version is available at: 11583/2920754 since: 2021-09-03T07:59:18Z

Publisher:

Springer

Published

DOI:10.1007/s11538-021-00914-3

Terms of use:

This article is made available under terms and conditions as specified in the corresponding bibliographic description in the repository

Publisher copyright

(Article begins on next page)



A Mathematical Study of the Influence of Hypoxia and Acidity on the Evolutionary Dynamics of Cancer

Giada Fiandaca¹ · Marcello Delitala¹ · Tommaso Lorenzi¹ 

Received: 24 August 2020 / Accepted: 25 May 2021 / Published online: 15 June 2021
© The Author(s) 2021

Abstract

Hypoxia and acidity act as environmental stressors promoting selection for cancer cells with a more aggressive phenotype. As a result, a deeper theoretical understanding of the spatio-temporal processes that drive the adaptation of tumour cells to hypoxic and acidic microenvironments may open up new avenues of research in oncology and cancer treatment. We present a mathematical model to study the influence of hypoxia and acidity on the evolutionary dynamics of cancer cells in vascularised tumours. The model is formulated as a system of partial integro-differential equations that describe the phenotypic evolution of cancer cells in response to dynamic variations in the spatial distribution of three abiotic factors that are key players in tumour metabolism: oxygen, glucose and lactate. The results of numerical simulations of a calibrated version of the model based on real data recapitulate the eco-evolutionary spatial dynamics of tumour cells and their adaptation to hypoxic and acidic microenvironments. Moreover, such results demonstrate how nonlinear interactions between tumour cells and abiotic factors can lead to the formation of environmental gradients which select for cells with phenotypic characteristics that vary with distance from intra-tumour blood vessels, thus promoting the emergence of intra-tumour phenotypic heterogeneity. Finally, our theoretical findings reconcile the conclusions of earlier studies by showing that the order in which resistance to hypoxia and resistance to acidity arise in tumours depend on the ways in which oxygen and lactate act as environmental stressors in the evolutionary dynamics of cancer cells.

This work was supported by the MIUR Grant “Dipartimenti di Eccellenza 2018–2022”.

✉ Tommaso Lorenzi
tommaso.lorenzi@polito.it

Giada Fiandaca
giada.fiandaca@polito.it

Marcello Delitala
marcello.delitala@polito.it

¹ Department of Mathematical Sciences “G. L. Lagrange”, Politecnico di Torino, Corso Duca degli Abruzzi, 24, Torino, Italy

Keywords Mathematical oncology · Intra-tumour heterogeneity · Eco-evolutionary dynamics · Vascularised tumours · Partial integro-differential equations

1 Introduction

Cancer is a dynamic disease, the characteristics of which are constantly evolving. This is reflected in the fact that the genotypic and phenotypic properties of cancer cells may change across space and time within the same tumour, and the dynamics of tumours with the same histological features are still likely to vary across patients. Moreover, since the same cancer clones may arise through different evolutionary pathways, the fact that two tumours have a similar clonal composition at a given point in time does not necessarily indicate that they share similar evolutionary histories, and does not rule out the possibility that their future evolution will diverge significantly (Maley et al. 2017). These sources of variability within and between tumours provide the substrate for the emergence and development of intra- and inter-tumour heterogeneity, which are major obstacles to cancer eradication (Gillies et al. 2012; Marusyk et al. 2012).

Clinical evidence suggests that cancer cells and the tumour microenvironment mutually shape each other (Gallaher et al. 2019). This supports the idea that tumours can be seen as evolving ecosystems where cancer cells with different phenotypic characteristics proliferate, die, undergo genotypic and phenotypic changes, and compete for space and resources under the selective pressure exerted by the various components of the tumour microenvironment (Gallaher and Anderson 2016; Gay et al. 2016; Ibrahim-Hashim et al. 2017; Korolev et al. 2014; Lloyd et al. 2016; Loeb 2001; Merlo et al. 2006; Michor and Polyak 2010; Villa et al. 2021; Vander Linden and Corbet 2020). In this light, intra-tumour phenotypic heterogeneity can be regarded as the outcome of an eco-evolutionary process in which spatial variability of the concentration of abiotic factors (i.e. substrates and metabolites) across the tumour supports the formation of distinct ecological niches whereby cells with different phenotypic characteristics may be selected (Casciari et al. 1992; Gatenby et al. 2007; Hockel and Vaupel 2001).

In normal tissues, cells produce the energy required to sustain their proliferation via oxidative phosphorylation (i.e. they rely on oxygen as their primary source of energy) and turn to glycolysis only when oxygen is scarce. In tumours, the presence of hypoxic regions (i.e. regions where the oxygen levels are below the physiological ones) induces cells to transiently switch to a glycolytic metabolic phenotype (i.e. to rely on glucose as their primary source of energy) (Vaupel et al. 2001). Cancer cells eventually acquire such a glycolytic phenotype and express it also in aerobic conditions, leading to the so-called Warburg effect (Kim and Dang 2006). The interplay between the high glycolytic rate of cancer cells and low perfusion in tumours brings about accumulation of lactate (i.e. a waste product of glycolysis), which causes acidity levels in the tumour microenvironment to rise (i.e. the pH level drops) (Tang et al. 2012).

Since hypoxia and acidity act as environmental stressors promoting selection for cancer cells with a more aggressive phenotype (Robertson-Tessi et al. 2015; Tang et al. 2012), an in-depth theoretical understanding of the spatio-temporal processes that drive the adaptation of tumour cells to hypoxic and acidic microenvironments may open up new avenues of research in oncology and cancer treatment (Martinez-Outschoorn

et al. 2016). In this regard, mathematical models can be an important source of support to cancer research, as they enable extrapolation beyond scenarios which can be investigated through experiments and may reveal emergent phenomena that would otherwise remain unobserved (Anderson and Quaranta 2008; Byrne 2010; Chaplain 2020; Chisholm et al. 2016; Eastman et al. 2020; Hamis and Powathil 2020; Poleszczuk et al. 2015). For instance, in their pioneering paper (Gatenby and Gawlinski 1996), Gatenby and Gawlinski used a reaction–diffusion system to explore how nonlinear interactions between cancer cells and abiotic components of the tumour microenvironment may shape tumour growth. The Gatenby–Gawlinski model has recently been extended in Strobl et al. (2020), in order to take into account the presence of cells with different phenotypic characteristics within the tumour. Hybrid cellular automaton models have been employed to study the impact of hypoxia and acidity on tumour growth and invasion (Anderson et al. 2006, 2009; Gatenby et al. 2007; Hatzikirou et al. 2012; Kim et al. 2018; Robertson-Tessi et al. 2015). A mechanical model of tumour growth whereby cells are allowed to switch between aerobic and anaerobic metabolism was presented in Astanin and Preziosi (2009). Integro-differential equations and partial integro-differential have been used in Ardaševa et al. (2020a), Chaplain et al. (2021), Lorenzi et al. (2018), Lorz et al. (2015), Villa et al. (2021) to investigate the ecological role of hypoxia in the development of intra-tumour phenotypic heterogeneity.

In this paper, we complement these earlier studies by presenting a mathematical model to study the influence of hypoxia and acidity on the evolutionary dynamics of cancer cells in vascularised tumours. The model comprises a system of partial integro-differential equations that describe the phenotypic evolution of cancer cells in response to dynamic variations in the spatial distribution of three abiotic factors that are key players in tumour metabolism: oxygen, glucose and lactate.

The remainder of the paper is organised as follows: In Sect. 2, we present the model equations and the underlying modelling assumptions. In Sect. 3, we summarise the main results of numerical simulations of the model and discuss their biological implications. Section 4 concludes the paper and provides a brief overview of possible research perspectives.

2 Model Description

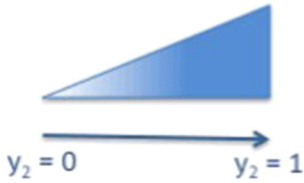
We consider a one-dimensional region of vascularised tissue of length $L > 0$. We describe the spatial position of every tumour cell in the tissue region by a scalar variable $x \in [0, L]$, and we assume a blood vessel to be present at $x = 0$ (cf. the schematic in Fig. 1a). Moreover, building upon the modelling framework developed in Chaplain et al. (2021), Lorenzi et al. (2018), Lorz et al. (2015), Villa et al. (2021), we model the phenotypic state of every cell by a vector $\mathbf{y} = (y_1, y_2) \in [0, 1]^2$ (cf. the schematics in Fig. 1b). Here, $y_1 \in [0, 1]$ represents the normalised level of expression of an acidity-resistant gene (e.g. the LAMP2 gene), while $y_2 \in [0, 1]$ represents the normalised level of expression of a hypoxia-resistant gene (e.g. the GLUT-1 gene) (Damaghi et al. 2015; Gatenby et al. 2007).

We describe the phenotypic distribution of tumour cells at position x and time $t \in [0, T]$, with $T > 0$, by means of the local population density function $n(t, x, \mathbf{y})$

(a) **Blood vessel**



(b) **Resistance to hypoxia**



Resistance to acidosis

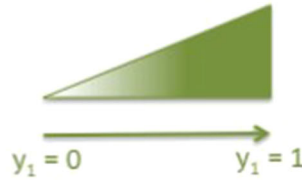


Fig. 1 **a** Schematic of the spatial domain defined as a one-dimensional region of vascularised tissue of length L . A blood vessel is assumed to be present at $x = 0$. **b** Schematics illustrating the relationships between the values of the variables y_2 and y_1 modelling the phenotypic state of tumour cells and the levels of resistance to hypoxia and acidosis (Color figure online)

(i.e. the local phenotypic distribution of tumour cells). We define the cell density $\rho(t, x)$, the local mean level of expression of the acidity-resistant gene $\mu_1(t, x)$ and the local mean level of expression of the hypoxia-resistant gene $\mu_2(t, x)$ as

$$\rho(t, x) := \int_{[0,1]^2} n(t, x, \mathbf{y}) \, d\mathbf{y}, \quad \mu_i(t, x) := \frac{1}{\rho(t, x)} \int_{[0,1]^2} y_i n(t, x, \mathbf{y}) \, d\mathbf{y} \quad (1)$$

for $i = 1, 2$. Moreover, we define the phenotypic distribution of tumour cells across the whole tissue region $f(t, \mathbf{y})$ as the mean value of $n(t, x, \mathbf{y})$ on the interval $[0, L]$, i.e.

$$f(t, \mathbf{y}) := \frac{1}{L} \int_0^L n(t, x, \mathbf{y}) \, dx. \quad (2)$$

Similarly, we define the levels of expression of the acidity-resistant gene and the hypoxia-resistant gene across the whole tissue region as the mean values of $\mu_1(t, x)$ and $\mu_2(t, x)$ on the interval $[0, L]$, respectively, i.e.

$$v_1(t) := \frac{1}{L} \int_0^L \mu_1(t, x) \, dx \quad \text{and} \quad v_2(t) := \frac{1}{L} \int_0^L \mu_2(t, x) \, dx. \quad (3)$$

The local concentrations of oxygen, glucose and lactate at position x and time t are denoted by $S_o(t, x)$, $S_g(t, x)$ and $S_l(t, x)$, respectively.

2.1 Dynamics of Tumour Cells

We describe the dynamics of tumour cells through the following balance equation for the local population density function $n(t, x, \mathbf{y})$

$$\frac{\partial n}{\partial t} = \underbrace{\beta_n \frac{\partial^2 n}{\partial x^2}}_{\text{undirected, random cell movement}} + \underbrace{\theta \Delta_{\mathbf{y}} n}_{\text{spontaneous phenotypic changes}} + \underbrace{R(S_o, S_g, S_l, \rho, \mathbf{y}) n}_{\text{proliferation and death}}, \tag{4}$$

with $(t, x, \mathbf{y}) \in (0, T] \times (0, L) \times (0, 1)^2$, subject to suitable initial conditions. We complement (4) with zero-flux boundary conditions at $x = 0$ and $x = L$ (i.e. we assume that cells cannot leave the tissue region) and zero-flux boundary conditions on the boundary of the square $[0, 1]^2$ (i.e. we assume that cells cannot have normalised levels of gene expression smaller than 0 or larger than 1).

The first term on the right-hand side of the partial integro-differential equation (4) models the effect of undirected, random movement, which is described through Fick’s first law of diffusion with diffusivity $\beta_n > 0$.

The second term on the right-hand side of the partial integro-differential equation (4) models the effect of heritable, spontaneous phenotypic changes, which occur at rate $\theta > 0$. Similar diffusion terms have been used in a number of previous papers to model the effect of spontaneous phenotypic changes (Alfaro and Veruete 2019; Almeida et al. 2019; Ardaševa et al. 2020b; Bouin et al. 2012; Chisholm et al. 2015; Iglesias and Mirrahimi 2018; Genieys et al. 2006; Lorenzi et al. 2016; Mirrahimi and Gandon 2020; Perthame and Génieys 2007) and can be obtained as the deterministic continuum limit of corresponding stochastic individual-based models in the asymptotic regime of large numbers of individuals and small phenotypic changes (Champagnat et al. 2006; Chisholm et al. 2016).

The function $R(S_o, S_g, S_l, \rho, \mathbf{y})$ represents the fitness of tumour cells in the phenotypic state \mathbf{y} at position x and time t under the environmental conditions given by the concentrations of abiotic factors $S_o(t, x)$, $S_g(t, x)$ and $S_l(t, x)$, and the cell density $\rho(t, x)$ (i.e. $R(S_o, S_g, S_l, \rho, \mathbf{y})$ is the phenotypic fitness landscape of the tumour). We use the following definition

$$R(S_o, S_g, S_l, \rho, \mathbf{y}) := \underbrace{P(S_o, S_g, y_2)}_{\substack{\text{proliferation and} \\ \text{death due to} \\ \text{oxygen-driven selection}}} - \underbrace{D(S_l, y_1)}_{\substack{\text{death due to} \\ \text{lactate-driven selection}}} - \underbrace{d(\rho)}_{\substack{\text{death due to} \\ \text{competition} \\ \text{for space}}}. \tag{5}$$

Here, the function $P(S_o, S_g, y_2)$ is the rate at which cells with level of expression y_2 of the hypoxia-resistant gene proliferate via oxidative phosphorylation and glycolysis and die due to oxygen-driven selection (i.e. $P(S_o, S_g, y_2)$ is a net proliferation rate). The function $D(S_l, y_1)$ is the rate at which cells with level of expression y_1 of the acidity-resistant gene die due to lactate-driven selection. The function $d(\rho)$ models the rate of cell death due to competition for space associated with saturation of the cell density.

2.1.1 Modelling Oxygen-Driven Selection

Based on the theoretical results and experimental data presented in Korolev et al. (2014), Vaupel et al. (2001), we focus on a scenario corresponding to the following biological assumptions.

Assumption 1 There exist two threshold levels of the oxygen concentration $O_M > O_m > 0$ such that the environment surrounding the cells is: hypoxic if $S_o \leq O_m$; moderately oxygenated if $O_m < S_o < O_M$; normoxic (i.e. well oxygenated) if $S_o \geq O_M$.

Assumption 2 Cells proliferate at a rate that depends on the concentrations of oxygen and glucose. Moreover, the trade-off between increase in cell death associated with sensitivity to hypoxia and decrease in cell proliferation associated with acquisition of resistance to hypoxia results in the existence of a level of expression of the hypoxia-resistant gene which is the fittest in that: a lower level of gene expression would correlate with a lower resistance to hypoxia and thus a higher death rate; a higher level of gene expression would correlate with a larger fitness cost and thus a lower proliferation rate. Cells with levels of gene expression that are closer to the fittest one are more likely to survive than the others. Hence, the farther the gene expression level of a cell is from the fittest one, the more likely is that the cell will die due to a form of oxygen-driven selection.

Assumption 3 In normoxic environments (i.e. when $S_o \geq O_M$), the energy required for cell proliferation is produced via oxidative phosphorylation and the cell proliferation rate is a monotonically increasing function of the concentration of oxygen. In hypoxic environments (i.e. when $S_o \leq O_m$), the energy required for cell proliferation is produced via glycolysis and the cell proliferation rate is a monotonically increasing function of the concentration of glucose. In moderately oxygenated environments (i.e. when $O_m < S_o < O_M$), the energy required for cell proliferation is produced via both oxidative phosphorylation and glycolysis. Moreover, the cell proliferation rate is a monotonically increasing function of the concentrations of oxygen and glucose, and lower values of the oxygen concentration correlate with a greater tendency of the cells to proliferate via glycolysis.

Assumption 4 The fittest level of expression of the hypoxia-resistant gene (i.e. the gene associated with the variable y_2) may vary with the oxygen concentration. In particular: in normoxic environments (i.e. when $S_o \geq O_M$), the fittest level of gene expression is the minimal one (i.e. $y_2 = 0$); in hypoxic environments (i.e. when $S_o \leq O_m$) the fittest level of gene expression is the maximal one (i.e. $y_2 = 1$); in moderately oxygenated environments (i.e. when $O_m < S_o < O_M$), the fittest level of gene expression is a monotonically decreasing function of the oxygen concentration (i.e. it decreases from $y_2 = 1$ to $y_2 = 0$ when the oxygen concentration increases).

Under Assumptions 1 and 2, we define the net proliferation rate $P(S_o, S_g, y_2)$ as

$$P(S_o, S_g, y_2) := \underbrace{p_o(S_o)}_{\text{proliferation via oxidative phosphorylation}} + \underbrace{p_g(S_o, S_g)}_{\text{proliferation via glycolysis}} - \underbrace{\eta_o (y_2 - \varphi_o(S_o))^2}_{\text{death due to oxygen-driven selection}}. \quad (6)$$

In (6), the function $p_o(S_o)$ models the rate of cell proliferation via oxidative phosphorylation, while the function $p_g(S_o, S_g)$ models the rate of cell proliferation via glycolysis. Furthermore, the third term in the definition given by (6) is the rate of death induced by oxygen-driven selection. Here, the parameter $\eta_o > 0$ is a selection gradient that quantifies the intensity of oxygen-driven selection and the function $\varphi_o(S_o)$ is the fittest level of expression of the hypoxia-resistant gene under the environmental conditions given by the oxygen concentration S_o .

Remark 1 In (6), the distance between y_2 and $\varphi_o(S_o)$ is computed as $(y_2 - \varphi_o(S_o))^2$. Alternatively, one could compute such a distance as $|y_2 - \varphi_o(S_o)|$. However, we have chosen $(y_2 - \varphi_o(S_o))^2$ over $|y_2 - \varphi_o(S_o)|$ because, as discussed in Ardaševa et al. (2020a), Lorenzi et al. (2016), it leads to a smoother fitness function which is closer to the approximate fitness landscapes which can be inferred from experimental data through regression techniques.

Under Assumptions 3 and 4, we use the definitions of the functions $p_o(S_o)$, $p_g(S_o, S_g)$ and $\varphi_o(S_o)$ given hereafter

$$p_o(S_o) := \frac{\gamma_o S_o}{\alpha_o + S_o} w(S_o), \quad p_g(S_o, S_g) := \frac{\gamma_g S_g}{\alpha_g + S_g} (1 - w(S_o)), \quad (7)$$

with

$$w(S_o) := \begin{cases} 1 & S_o \geq O_M \\ 1 - \frac{O_M - S_o}{O_M - O_m} & O_m < S_o < O_M \\ 0 & S_o \leq O_m \end{cases} \quad (8)$$

and

$$\varphi_o(S_o) := \begin{cases} 0 & S_o \geq O_M \\ \frac{O_M - S_o}{O_M - O_m} & O_m < S_o < O_M \\ 1 & S_o \leq O_m. \end{cases} \quad (9)$$

In (7), the parameters $\gamma_o > 0$ and $\gamma_g > 0$ model the maximum rates of cell proliferation via oxidative phosphorylation and glycolysis, respectively. The parameters $\alpha_o > 0$ and $\alpha_g > 0$ are the Michaelis–Menten constants of oxygen and glucose. The weight function $w(S_o)$ defined via (8) ensures that Assumption 3 is satisfied, while definition (9) of $\varphi_o(S_o)$ is such that Assumption 4 is satisfied (cf. the plot in Fig. 2a).

2.1.2 Modelling Lactate-Driven Selection

Based on theoretical results and experimental data presented in Robertson-Tessi et al. (2015), we focus on a scenario corresponding to the following biological assumptions.

Assumption 5 There exist two threshold levels of the lactate concentration $L_M > L_m > 0$ such that the environment surrounding the cells is: mildly acidic if $S_l \leq L_m$; moderately acidic if $L_m < S_l < L_M$; highly acidic if $S_l \geq L_M$.

Assumption 6 Cells die at a rate that depends on the concentration of lactate. Moreover, the trade-off between increase in cell death associated with sensitivity to acidity and decrease in cell proliferation associated with acquisition of resistance to acidity results in the existence of a level of expression of the acidity-resistant gene which is the fittest in that: a lower level of gene expression would correlate with a lower resistance to acidity and thus a higher death rate; a higher level of gene expression would correlate with a larger fitness cost and thus a lower proliferation rate. Cells with levels of gene expression that are closer to the fittest one are more likely to survive than the others. Hence, the farther the gene expression level of a cell is from the fittest one, the more likely is that the cell will die due to a form of lactate-driven selection.

Assumption 7 The fittest level of expression of the acidity-resistant gene (i.e. the gene associated with the variable y_1) may vary with the lactate concentration. In particular: in mildly acidic environments (i.e. when $S_l \leq L_m$), the fittest level of gene expression is the minimal one (i.e. $y_1 = 0$); in highly acidic environments (i.e. when $S_l \geq L_M$) the fittest level of gene expression is the maximal one (i.e. $y_1 = 1$); in moderately acidic environments (i.e. when $L_m < S_l < L_M$), the fittest level of gene expression is a monotonically increasing function of the lactate concentration (i.e. it increases from $y_1 = 0$ to $y_1 = 1$ when the lactate concentration increases).

Under Assumptions 5 and 6, we define the rate of cell death due to lactate-driven selection $D(S_l, y_1)$ as

$$D(S_l, y_1) := \eta_l (y_1 - \varphi_l(S_l))^2. \quad (10)$$

In (10), the parameter $\eta_l > 0$ is a selection gradient that quantifies the intensity of lactate-driven selection and the function $\varphi_l(S_l)$ is the fittest level of expression of the acidity-resistant gene under the environmental conditions given by the lactate concentration S_l . Considerations analogous to those made in Remark 1 on the term $(y_2 - \varphi_o(S_o))^2$ in (6) apply to the term $(y_1 - \varphi_l(S_l))^2$ in (10). Finally, we use the definition of the function $\varphi_l(S_l)$ given hereafter (cf. the plot in Fig. 2b), so that Assumption 7

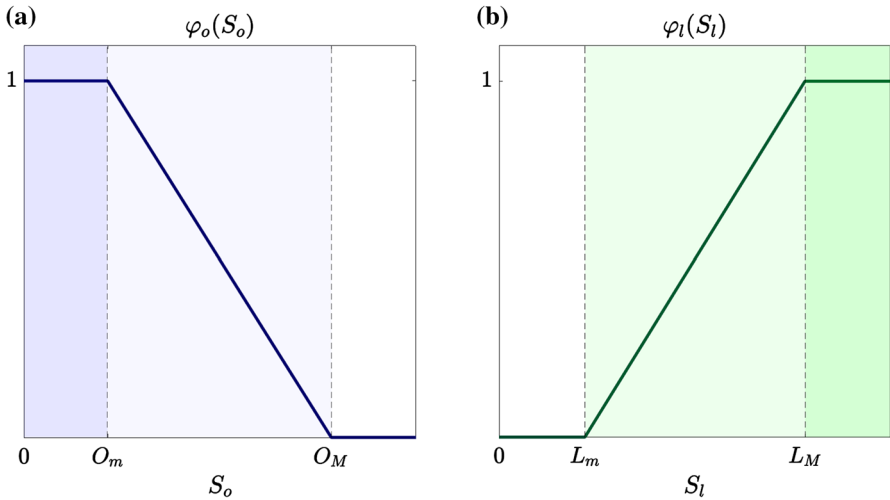


Fig. 2 **a** Plot of the fittest level of expression of the hypoxia-resistant gene $\varphi_o(S_o)$ defined via (9). The vertical, dashed lines highlight the oxygen levels O_m and O_M . Hence, the white region corresponds to normoxic conditions, the pale-blue region corresponds to moderately oxygenated environments and the blue region corresponds to hypoxic conditions. **b** Plot of the fittest level of expression of the acidity-resistant gene $\varphi_l(S_l)$ defined via (11). The vertical, dashed lines highlight the lactate levels L_m and L_M . Hence, the white region corresponds to mildly acidic conditions, the pale-green region corresponds to moderately acidic conditions and the green region corresponds to highly acidic conditions (Color figure online)

is satisfied:

$$\varphi_l(S_l) := \begin{cases} 0 & S_l \leq L_m \\ \frac{S_l - L_m}{L_M - L_m} & L_m < S_l < L_M \\ 1 & S_l \geq L_M. \end{cases} \tag{11}$$

2.1.3 Modelling Competition for Space

We define the rate of cell death due to competition for space associated with saturation of the cell density as

$$d(\rho) := \kappa \rho. \tag{12}$$

Here, the proportionality constant $\kappa > 0$ is related to the local carrying capacity of the tumour, which may vary depending on the tumour type.

2.2 Dynamics of Abiotic Factors

Oxygen and glucose are consumed by tumour cells, while lactate is produced by tumour cells as a waste product of glycolysis. Moreover, oxygen, glucose and lactate diffuse in space and decay over time. Hence, their dynamics are governed by the following balance equations for the functions $S_o(t, x)$, $S_g(t, x)$ and $S_l(t, x)$, respectively,

$$\frac{\partial S_o}{\partial t} = \underbrace{\beta_o \frac{\partial^2 S_o}{\partial x^2}}_{\text{diffusion}} - \underbrace{\lambda_o S_o}_{\text{natural decay}} - \underbrace{\zeta_o p_o(S_o) \rho}_{\text{consumption by tumour cells}}, \quad (13)$$

$$\frac{\partial S_g}{\partial t} = \underbrace{\beta_g \frac{\partial^2 S_g}{\partial x^2}}_{\text{diffusion}} - \underbrace{\lambda_g S_g}_{\text{natural decay}} - \underbrace{\zeta_g p_g(S_o, S_g) \rho}_{\text{consumption by tumour cells}} \quad (14)$$

and

$$\frac{\partial S_l}{\partial t} = \underbrace{\beta_l \frac{\partial^2 S_l}{\partial x^2}}_{\text{diffusion}} - \underbrace{\lambda_l S_l}_{\text{natural decay}} + \underbrace{\zeta_l p_g(S_o, S_g) \rho}_{\text{production by tumour cells}}, \quad (15)$$

with $(t, x) \in (0, T] \times (0, L)$, subject to suitable boundary conditions (see considerations below) and initial conditions.

In (13)–(15), the parameters $\beta_o > 0$, $\beta_g > 0$ and $\beta_l > 0$ are the diffusion coefficients of oxygen, glucose and lactate, respectively, while the parameters $\lambda_o > 0$, $\lambda_g > 0$ and $\lambda_l > 0$ are the natural decay rates of the three abiotic factors. The third term on the right-hand side of (13) is the consumption rate of oxygen by tumour cells, which is proportional to the product between the cell density ρ and the rate of cell proliferation via oxidative phosphorylation $p_o(S_o)$, which is defined via (7). The parameter $\zeta_o > 0$ is a conversion factor linked to oxygen consumption by the cells. Analogous considerations hold for the third term on the right-hand side of (14), which models the consumption rate of glucose by tumour cells. Furthermore, the third term on the right-hand side of (15) is the production rate of lactate by tumour cells, which is assumed to be proportional to the product between the cell density ρ and the rate of cell proliferation via glycolysis $p_g(S_o, S_g)$ defined via (7). The constant of proportionality is the conversion factor $\zeta_l > 0$ linked to lactate production by the cells.

We assume that oxygen and glucose enter the spatial domain through the blood vessel only, while lactate is flushed out through the blood vessel only. Hence, focussing on the case where the inflow rate of oxygen and glucose and the outflow rate of lactate are constant, we complement (13)–(15) with the following boundary conditions at $x = 0$

$$S_o(t, 0) = \bar{S}_o, \quad S_g(t, 0) = \bar{S}_g, \quad S_l(t, 0) = \underline{S}_l \quad \text{for all } t > 0, \quad (16)$$

where $\bar{S}_o > 0$ and $\bar{S}_g > 0$ are related to the average physiological levels of oxygen and glucose in proximity to blood vessels, while $\underline{S}_l > 0$ is a small parameter of value close

to zero. In particular, we have $\bar{S}_o > O_M$ and $\underline{S}_l < L_m$. Moreover, we assume that far from the blood vessel the concentrations of oxygen and glucose drop to some lower values $0 < \underline{S}_o < \bar{S}_o$ and $0 < \underline{S}_g < \bar{S}_g$, which correspond to the levels of oxygen and glucose, which are typically observed in regions distant from blood vessels. In particular, we have $\underline{S}_o < O_m$. Furthermore, we model abnormal accumulation of lactate, which is expected to occur far from blood vessels, imposing zero-flux boundary conditions. Therefore, we complement (13)–(15) with the following boundary conditions at $x = L$

$$S_o(t, L) = \underline{S}_o, \quad S_g(t, L) = \underline{S}_g, \quad \frac{\partial S_l(t, L)}{\partial x} = 0 \quad \text{for all } t > 0. \quad (17)$$

3 Main Results

In this section, we present the results of numerical simulations of the mathematical model defined by (4) coupled with (13)–(15) and we discuss their biological relevance. First, we describe the set-up of numerical simulations (see Sect. 3.1). Next, we present a sample of numerical solutions that summarise the spatial dynamics of tumour cells and abiotic factors (see Sect. 3.2). Then, we report on the results of numerical simulations showing the evolutionary dynamics of tumour cells and the emergence of phenotypic heterogeneity (see Sect. 3.3). Finally, we present the results of numerical simulations that reveal the existence of alternative evolutionary pathways that may lead to the development of resistance to hypoxia and acidity in vascularised tumours (see Sect. 3.4).

3.1 Set-Up of Numerical Simulations

Numerical simulations are carried out assuming $L = 400 \mu m$, which is chosen coherently with experimental data reported in Molavian et al. (2009), and $t \in [0, T]$, where the final time $T > 0$ is such that the solutions of the model equations are at numerical equilibrium for $t = T$.

Initial Conditions We consider (13), (14) and (15) subject, respectively, to the following initial conditions

$$S_o(0, x) = S_o^0(x), \quad S_g(0, x) = S_g^0(x) \quad \text{and} \quad S_l(0, x) = S_l^0(x) \equiv \underline{S}_l. \quad (18)$$

Here, the functions $S_o^0(x)$ and $S_g^0(x)$ (see Fig. 3) are defined in such a way as to match the experimental equilibrium distributions of oxygen and glucose presented in Molavian et al. (2009, Fig. 2), while \underline{S}_l is the same small parameter used in (16), i.e. $\underline{S}_l < L_m$. Initial conditions (18) correspond to a situation in which the initial distributions of oxygen and glucose match with experimental equilibrium distributions of such abiotic factors and lactate is present at a uniform level which is below the threshold level L_m , that is, the level below which the environment surrounding the cells is mildly acidic and the fittest level of expression of the acidity-resistant gene is

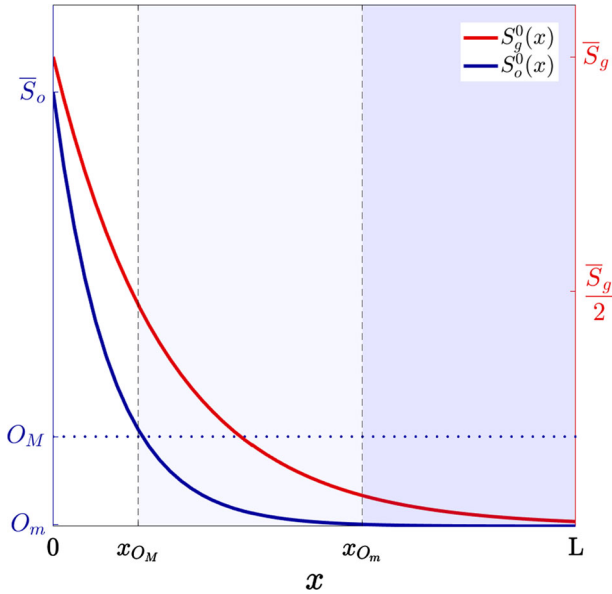


Fig. 3 Plots of the initial distribution of oxygen $S_o^0(x)$ (blue curve, axis on the left) and the initial distribution of glucose $S_g^0(x)$ (red curve, axis on the right) which are defined in such a way as to match the experimental equilibrium distributions of oxygen and glucose presented in Molavian et al. (2009, Fig. 2). The vertical, dashed lines highlight the points x_{O_M} and x_{O_m} such that $S_o^0(x_{O_M}) = O_M$ and $S_o^0(x_{O_m}) = O_m$. Hence, the white region corresponds to normoxic conditions, the pale-blue region corresponds to moderately oxygenated environments and the blue region corresponds to hypoxic conditions (Color figure online)

the minimal one. Moreover, we complement (4) with the following initial condition

$$n(0, x, y) = n^0(x, y) := 200 \exp\left(-\frac{(x - 0)^2}{0.0002} - \frac{|y - 0|^2}{0.4}\right), \tag{19}$$

which corresponds to a biological scenario in which at the initial time $t = 0$ most tumour cells are concentrated near the blood vessel and are characterised by the minimal expression level of both the hypoxia-resistant gene and the acidity-resistant gene.

Boundary Conditions We use the following values of the parameters \bar{S}_o , \bar{S}_g and \underline{S}_l in (16)

$$\bar{S}_o = 2.08 \times 10^{-6} \text{ g/cm}^3, \quad \bar{S}_g = 1.35 \times 10^{-4} \text{ g/cm}^3, \quad \underline{S}_l = 10^{-8} \text{ g/cm}^3 \tag{20}$$

and the following values of the parameters \underline{S}_o and \underline{S}_g in (17)

$$\underline{S}_o = 2 \times 10^{-10} \text{ g/cm}^3, \quad \underline{S}_g = 1.35 \times 10^{-6} \text{ g/cm}^3. \tag{21}$$

The values of \bar{S}_o and \bar{S}_g correspond to the average physiological levels of oxygen and glucose in proximity to blood vessels reported in Molavian et al. (2009). Moreover,

the values of \underline{S}_o and \underline{S}_g correspond to the 0.1% of \bar{S}_o and the 1% of \bar{S}_g , respectively. This is because, based on experimental data reported in Molavian et al. (2009), we expect the concentrations of oxygen and glucose at $400 \mu m$ from the blood vessel (i.e. at $x = L$) to drop, respectively, below the 0.1% and the 1% of their value near the blood vessel.

Parameter Values Unless otherwise explicitly stated, we use the values of the model parameters listed in Table 1, which are chosen to be consistent with the existing literature, except for the values of the parameters η_o , η_l , λ_l and ζ_l that are model specific in that we could not find them in the literature and are defined on the basis of the following considerations. The value of the conversion factor for lactate production ζ_l is chosen to be the same as the value of the conversion factor for glucose consumption ζ_g . Furthermore, the value of the rate of natural decay of lactate λ_l is such that the distribution of lactate at numerical equilibrium (i.e. the graph of $S_l(T, x)$) is similar to the lactate distributions reported in Molavian et al. (2009). Finally, although the values of the selection gradients η_o and η_l are chosen with exploratory aim, a systematic sensitivity analysis of the evolutionary dynamics of tumour cells to the values of these parameters was carried out, and the key findings from such sensitivity analysis are summarised by the results presented in Sect. 3.4. We also note that the value of the rate of phenotypic changes given in Table 1 is consistent with experimental data reported in Doerfler and Böhm (2006) and Duesberg et al. (2000).

Numerical Methods Numerical solutions are constructed using a uniform discretisation of the interval $[0, L]$ as the computational domain of the independent variable x and a uniform discretisation of the square $[0, 1]^2$ as the computational domain of the independent variable \mathbf{y} . We also discretise the interval $[0, T]$ with a uniform step. The method for constructing numerical solutions is based on an explicit finite difference scheme in which a three-point and a five-point stencils are used to approximate the diffusion terms in x and \mathbf{y} , respectively, and an implicit–explicit finite difference scheme is used for the reaction terms (LeVeque 2007; Lorz et al. 2013). All numerical computations are performed in MATLAB.

3.2 Dynamics of the Cell Density and the Concentrations of Abiotic Factors

The dynamics of the density of tumour cells and the concentrations of abiotic factors are illustrated by the plots in Fig. 4. In summary, the cell density and the concentration of lactate at successive times (i.e. the graphs of $\rho(t, x)$ for four different values of t and $S_l(t, x)$ for three different values of t) are displayed in Fig. 4a, c, respectively, while the concentrations of oxygen and glucose at time T (i.e. the graphs of $S_o(T, x)$ and $S_g(T, x)$) are displayed in Fig. 4b.

The dashed lines in Fig. 4 highlight the spatial positions x_{O_M} and x_{O_m} at which the oxygen concentration at time T crosses, respectively, the threshold values O_M and O_m (i.e. $S_o(T, x_{O_M}) = O_M$ and $S_o(T, x_{O_m}) = O_m$). Hence, the white region (i.e. the interval $[0, x_{O_M}]$), the pale-blue region (i.e. the interval (x_{O_M}, x_{O_m})) and the blue

Table 1 Parameter values used in numerical simulations

Par.	Biological meaning	Value	Units	References
β_o	Diffusion coefficient of oxygen	1.46×10^{-5}	$\text{cm}^2 \text{s}^{-1}$	Molavian et al. (2009)
β_g	Diffusion coefficient of glucose	1.10×10^{-6}	$\text{cm}^2 \text{s}^{-1}$	Molavian et al. (2009)
β_l	Diffusion coefficient of lactate	1.9×10^{-6}	$\text{cm}^2 \text{s}^{-1}$	Molavian et al. (2009)
β_n	Cell motility	10^{-13}	$\text{cm}^2 \text{s}^{-1}$	Villa et al. (2021)
θ	Rate of phenotypic changes	10^{-13}	s^{-1}	Villa et al. (2021)
λ_o	Rate of natural decay of oxygen	1.2×10^{-3}	s^{-1}	Molavian et al. (2009)
λ_g	Rate of natural decay of glucose	2.33×10^{-5}	s^{-1}	Molavian et al. (2009)
λ_l	Rate of natural decay of lactate	5×10^{-2}	s^{-1}	Ad hoc
γ_o	Max. prolif. rate via oxidative phosphorylation	3.65×10^{-7}	s^{-1}	Molavian et al. (2009)
α_o	Michaelis-Menten constant of oxygen	6.4×10^{-9}	g cm^{-3}	Molavian et al. (2009)
γ_g	Max. prolif. rate via glycolysis	3.42×10^{-7}	s^{-1}	Molavian et al. (2009)
α_g	Michaelis-Menten constant of glucose	9×10^{-6}	g cm^{-3}	Molavian et al. (2009)
η_o	Selection gradient related to oxygen	3.65×10^{-2}	s^{-1}	Ad hoc
η_l	Selection gradient related to lactate	10^{-2}	s^{-1}	Ad hoc
κ	Rate of cell death due to competition for space	2×10^{-10}	$\text{cm}^3 \text{s}^{-1} \text{cells}^{-1}$	Lorenzi et al. (2018)
ζ_o	Conversion factor for oxygen consumption	10^{-8}	g cells^{-1}	Lorenzi et al. (2018)
ζ_g	Conversion factor for glucose consumption	10^{-8}	g cells^{-1}	Lorenzi et al. (2018)
ζ_l	Conversion factor for lactate production	10^{-8}	g cells^{-1}	Ad hoc
O_m	Threshold level of oxygen for hypoxic env.	8.2×10^{-9}	g cm^{-3}	Vaupel et al. (2001)
O_M	Threshold level of oxygen for normoxic env.	4.3×10^{-7}	g cm^{-3}	Vaupel et al. (2001)
L_m	Threshold level of lactate for mildly acidic env.	2×10^{-5}	g cm^{-3}	Robertson-Tessi et al. (2015)
L_M	Threshold level of lactate for highly acidic env.	7.15×10^{-5}	g cm^{-3}	Robertson-Tessi et al. (2015)
L	Max. distance from blood vessel	400	μm	Molavian et al. (2009)

region (i.e. the interval $[x_{O_m}, L]$) correspond to normoxic, moderately oxygenated and hypoxic environmental conditions, respectively.

The curves in Fig. 4a summarise the evolution of the cell number density $\rho(t, x)$, which behaves like an invading front whereby growth is saturated at a value that decreases with the distance from the blood vessel (i.e. $\rho(t, x)$ converges to a form of generalised transition wave Berestycki and Hamel 2012; Berestycki and Nadin

2020). These results illustrate how the synergistic interaction between cell proliferation, which occurs until the local carrying capacity of the tissue is reached, and cell movement allows tumour cells, which are initially located in the proximity of the blood vessel, to invade the surrounding tissue. The result that the plateau value of the cell number density decreases with the distance from the blood vessel, which is a result with broad structural stability under parameter changes (see Appendix A), reflects the fact that, in our model, the cell proliferation rate in normoxic conditions, whereby the energy needed for cell proliferation is produced via oxidative phosphorylation, is higher than the cell proliferation rate in moderately oxygenated environments, which in turn is higher than the cell proliferation rate in hypoxic conditions, whereby the energy needed for cell proliferation is produced via glycolysis (cf. the blue curve in Fig. 5). This is in line with experimental evidence, indicating that glycolysis is less efficient than oxidative phosphorylation as a mechanism to produce the energy required for cell proliferation.

Moreover, the curves in Fig. 4b show how the reaction–diffusion dynamics of oxygen and glucose, along with the inflow through the blood vessel and the consumption by tumour cells, lead the concentrations of such abiotic factors to converge to some stable values, which decrease as the distance from the blood vessel increases (i.e. at $t = T$, $S_o(t, x)$ and $S_g(t, x)$ appear to be at numerical equilibrium and are monotonically decreasing functions of x). Notice that the distributions of oxygen and glucose at the final time T are close to the initial distributions $S_o^0(x)$ and $S_g^0(x)$ displayed in Fig. 3. This is to be expected. In fact, since $S_o^0(x)$ and $S_g^0(x)$ are defined in such a way as to match experimental equilibrium distributions of oxygen and glucose, under the biologically informed parameter values (cf. Table 1) and boundary conditions (cf. (16), (17) and (20), (21)) used here, the concentrations $S_o(t, x)$ and $S_g(t, x)$ reach quickly numerical equilibrium. We verified via additional numerical simulations (results not shown) that, as one would expect, the concentrations of oxygen and glucose at numerical equilibrium do not depend on the choice of the initial conditions.

Finally, the curves in Fig. 4c summarise the evolution of the concentration of lactate $S_l(t, x)$, which is the result of the interplay between the production of this abiotic factor by tumour cells, its reaction–diffusion dynamics and its outflow through the blood vessel. It is known that, as a waste product of glycolysis, lactate is mainly produced and accumulate in moderately oxygenated and hypoxic regions, where cell proliferation relies more on glycolysis and tissue perfusion is poorer. In agreement with this, the curves in Fig. 4c demonstrate that the concentration of lactate increases with the distance from the blood vessel. In particular, the values attained by $S_l(T, x)$, which depend on the values of the production rate of lactate in our model (cf. the red curve in Fig. 5), are in agreement with lactate concentrations reported in Molavian et al. (2009).

3.3 Evolutionary Dynamics of Tumour Cells and Emergence of Phenotypic Heterogeneity

As discussed in the previous section, reaction–diffusion dynamics of abiotic factors and mutual interactions between abiotic factors and tumour cells lead to the emergence

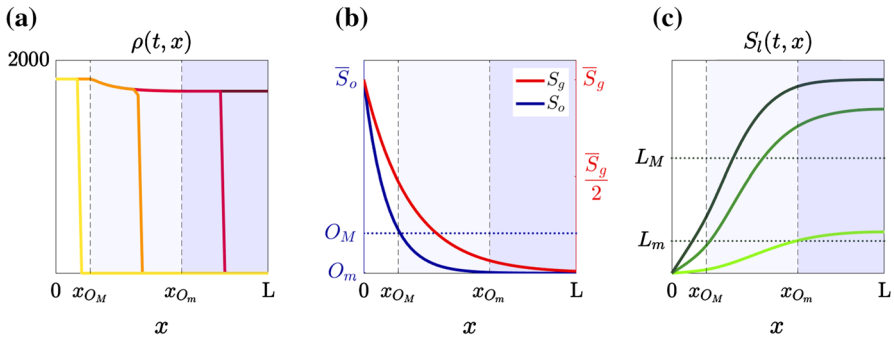


Fig. 4 **a** Plots of the cell density $\rho(t, x)$ at four successive time instants (yellow, orange, red and burgundy lines). The burgundy line highlights $\rho(T, x)$. **b** Plots of the concentrations of oxygen $S_o(T, x)$ (blue line) and glucose $S_g(T, x)$ (red line). **c** Plots of the concentration of lactate $S_l(T, x)$ at three successive time instants (light-green, green and dark-green lines). The dark-green line highlights $S_l(T, x)$. In every panel, the vertical, dashed lines highlight the points x_{O_M} and x_{O_m} such that $S_o(T, x_{O_M}) = O_M$ and $S_o(T, x_{O_m}) = O_m$. Hence, the white region corresponds to normoxic conditions, the pale-blue region corresponds to moderately oxygenated environments and the blue region corresponds to hypoxic conditions (Color figure online)

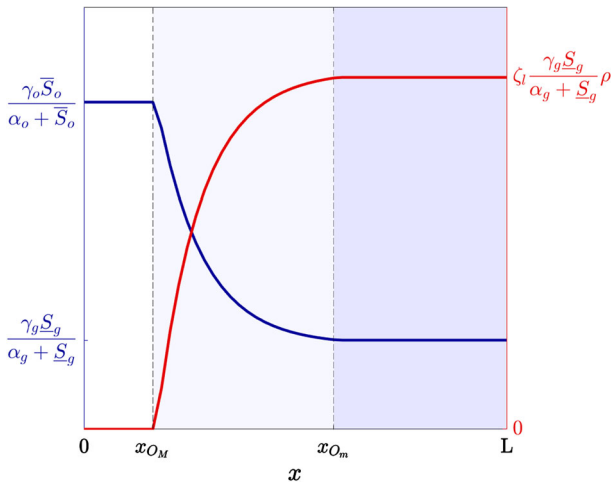


Fig. 5 Plots of the cell proliferation rate $p_o(S_o(T, x)) + p_g(S_o(T, x), S_g(T, x))$ (blue curve, axis on the left) and the production rate of lactate $\zeta_l p_g(S_o(T, x), S_g(T, x)) \rho(T, x)$ (red curve, axis on the right) defined via (7). The vertical, dashed lines highlight the points x_{O_M} and x_{O_m} such that $S_o(T, x_{O_M}) = O_M$ and $S_o(T, x_{O_m}) = O_m$. Hence, the white region corresponds to normoxic conditions, the pale-blue region corresponds to moderately oxygenated environments and the blue region corresponds to hypoxic conditions (Color figure online)

of spatial variations in the concentrations of oxygen and lactate—i.e. the oxygen concentration $S_o(T, x)$ is a monotonically decreasing function of x , while the lactate concentration $S_l(T, x)$ is a monotonically increasing function of x (cf. plots in Fig. 4b, c).

Spatial variability of oxygen and lactate concentrations can lead to the formation of environmental gradients resulting in the selection for cells with phenotypic charac-

teristics that vary with distance from the blood vessel, thus promoting the emergence of intra-tumour phenotypic heterogeneity. The numerical results displayed in Fig. 6 support the idea that this can be effectively captured by our model.

The dashed lines in Fig. 6a, b highlight the fittest levels of expression of the hypoxia-resistant gene (see Fig. 6a) and the acidity-resistant gene (see Fig. 6b) at time T [i.e. the graphs of $\varphi_o(S_o(T, x))$ and $\varphi_l(S_l(T, x))$], while the solid lines display the local mean levels of expression of the hypoxia-resistant gene (see Fig. 6a) and the acidity-resistant gene (see Fig. 6b) at four successive times (i.e. the graphs of $\mu_2(t, x)$ and $\mu_1(t, x)$ for four different values of t). In analogy with Fig. 4, the vertical, dashed lines in Fig. 6a highlight the spatial positions x_{O_M} and x_{O_m} at which the oxygen concentration at time T crosses, respectively, the threshold values O_M and O_m (i.e. $S_o(T, x_{O_M}) = O_M$ and $S_o(T, x_{O_m}) = O_m$). Hence, the white region corresponds to normoxic conditions, the pale-blue region corresponds to moderately oxygenated environments and the blue region corresponds to hypoxic conditions. Moreover, the vertical, dashed lines in Fig. 6b highlight the spatial positions x_{L_m} and x_{L_M} at which the lactate concentration at time T crosses, respectively, the threshold values L_m and L_M (i.e. $S_l(T, x_{L_m}) = L_m$ and $S_l(T, x_{L_M}) = L_M$). Hence, the white region corresponds to mildly acidic conditions, the pale-green region corresponds to moderately acidic conditions and the green region corresponds to highly acidic conditions.

As shown by the plots in Fig. 6a, b, the local mean levels of expression of the hypoxia- and acidity-resistant genes converge, as time passes, to the fittest ones (i.e. $\mu_2(T, x)$ matches with $\varphi_o(S_o(T, x))$ and $\mu_1(T, x)$ matches with $\varphi_l(S_l(T, x))$), the values of which vary with the distance from the blood vessel depending on the local concentrations of oxygen and lactate. In more detail, the local mean level of expression of the hypoxia-resistant gene at time T is the minimal one in normoxic conditions (i.e. $\mu_2(T, x) \equiv 0$ for $x \in [0, x_{O_M}]$), the maximal one in hypoxic conditions (i.e. $\mu_2(T, x) \equiv 1$ for $x \in [x_{O_m}, L]$) and increases with the oxygen concentration in moderately oxygenated environments (i.e. $\mu_2(T, x)$ increases monotonically from 0 to 1 for $x \in (x_{O_M}, x_{O_m})$). Furthermore, the local mean level of expression of the acidity-resistant gene at time T is the minimal one in the mildly acidic region (i.e. $\mu_1(T, x) \equiv 0$ for $x \in [0, x_{L_m}]$), the maximal one in highly acidic conditions (i.e. $\mu_1(T, x) \equiv 1$ for $x \in [x_{L_M}, L]$) and increases with the lactate concentration in moderately acidic environments (i.e. $\mu_1(T, x)$ increases monotonically from 0 to 1 for $x \in (x_{L_m}, x_{L_M})$). These are results with broad structural stability under parameter changes (see Appendix A).

Finally, the plots in Fig. 6c–e show that, at every position $x \in [0, L]$, the local phenotypic distribution of tumour cells at time T (i.e. the local population density function $n(T, x, \mathbf{y})$) is unimodal and attains its maximum at the fittest phenotypic state $\mathbf{y} = (\varphi_o(S_o(T, x)), \varphi_l(S_l(T, x)))$. As discussed in Appendix A, such a qualitative behaviour of $n(T, x, \mathbf{y})$ is in agreement with predictions based on the formal asymptotic results presented in Villa et al. (2021).

The numerical results of Fig. 6 are complemented by the numerical results displayed in Fig. 7, which summarise the time evolution of the phenotypic distribution of tumour cells across the whole tissue region (i.e. the function $f(t, \mathbf{y})$ defined via (2)) and show that the maximum point of the distribution departs from the point $\mathbf{y} = (0, 0)$ (i.e. the point corresponding to the minimal expression level of both the acidity-resistant gene

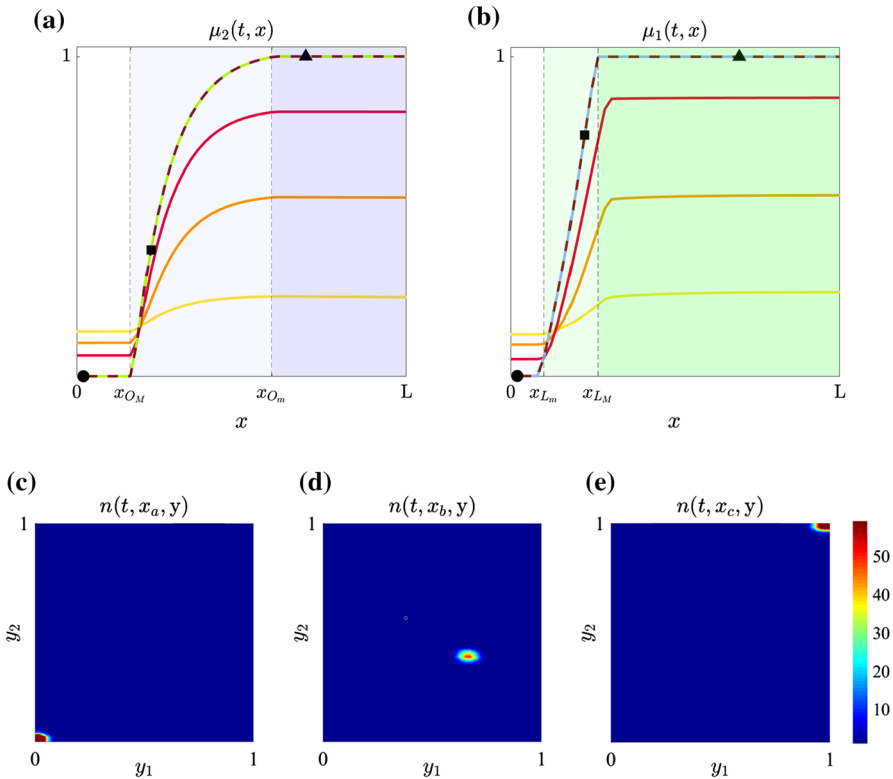


Fig. 6 **a** Plots of the normalised level of expression of the hypoxia-resistant gene $\mu_2(t, x)$ at four successive time instants (yellow, orange, red and light-green lines). The light-green line highlights $\mu_2(T, x)$ and the burgundy, dashed line highlights the fittest level of expression of the hypoxia-resistant gene $\varphi_o(S_o(T, x))$ defined via (9). The vertical, dashed lines highlight the points x_{O_M} and x_{O_m} such that $S_o(T, x_{O_M}) = O_M$ and $S_o(T, x_{O_m}) = O_m$. Hence, the white region corresponds to normoxic conditions, the pale-blue region corresponds to moderately oxygenated environments and the blue region corresponds to hypoxic conditions. **b** Plots of the normalised level of expression of the acidity-resistant gene $\mu_1(t, x)$ at four successive time instants (yellow, orange, red and light-blue lines). The light-blue line highlights $\mu_1(T, x)$, and the burgundy, dashed line highlights the fittest level of expression of the acidity-resistant gene $\varphi_l(S_l(T, x))$ defined via (11). The vertical, dashed lines highlight the points x_{L_m} and x_{L_M} such that $S_l(T, x_{L_m}) = L_m$ and $S_l(T, x_{L_M}) = L_M$. Hence, the white region corresponds to mildly acidic conditions, the pale-green region corresponds to moderately acidic conditions and the green region corresponds to highly acidic conditions. **c–e** Plots of the local phenotypic distribution of tumour cells $n(T, x, \mathbf{y})$ at the points $x = x_a$, $x = x_b$ and $x = x_c$ highlighted, respectively, by the circle, square and triangle markers shown in **a** and **b** (Color figure online)

and the hypoxia-resistant gene)—cf. the initial condition $n^0(x, \mathbf{y})$ defined via (19)—and moves toward the point $\mathbf{y} = (1, 1)$, which corresponds to the maximal expression level of both the hypoxia-resistant gene and the acidity-resistant gene (i.e. the degree of malignancy of the tumour increases over time).

These results recapitulate key ideas about the eco-evolutionary dynamics of tumour cells proposed in Maley et al. (2017) by demonstrating how patchy resources (i.e. oxygen and glucose) and hazards (i.e. the selective pressure effects of lactate), which define

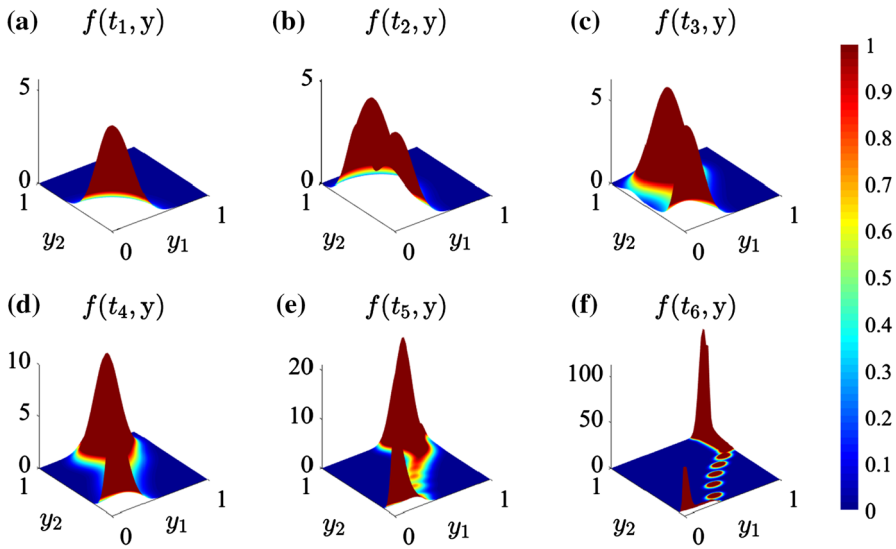


Fig. 7 Plots of the phenotypic distribution of tumour cells across the whole tissue region $f(t, y)$ defined according to (2) at six successive time instants $t_1 < t_2 < \dots < t_6$ (Color figure online)

the ecology of the tumour, can create multiple habitats whereby different phenotypic variants may be selected according to the principle of the “survival of the fittest” (i.e. through a functional trade-off between the ability to survive under certain environmental conditions and the evolutionary cost of acquiring such an ability). In the same vein, these results also support the idea that tumour growth can be conceptualised as an ecological process driven by consecutive phases of invasion and colonisation of new tissue habitats by tumour cells, which may be accelerated by the presence of gradients of abiotic factors corresponding to harsher environmental conditions.

3.4 Alternative Evolutionary Pathways Leading to the Development of Resistance to Hypoxia and Acidity

In line with the classification of the evolutionary and ecological features of neoplasms presented in Maley et al. (2017), the ratio between the selection gradients η_o and η_l of our model could be seen as a measure of the impact that hypoxia and acidity may have on the eco-evolutionary dynamics of tumour cells. Hence, in this section we explore how the dynamics of the levels of expression of the acidity-resistant gene and the hypoxia-resistant gene across the whole tissue region (i.e. the functions $v_1(t)$ and $v_2(t)$ defined via (3)) are affected by the value of the ratio η_o/η_l .

The plot in Fig. 8, which displays the curve $\phi(t) = (v_1(t), v_2(t))$, demonstrates that resistance to hypoxia and resistance to acidity arise via alternative evolutionary pathways depending on the value of η_o/η_l . Coherently with the results presented in the previous section, $\phi(t)$ departs from the point (0.15, 0.15) (i.e. the point corresponding to the initial levels of expression of the acidity-resistant gene and the hypoxia-resistant

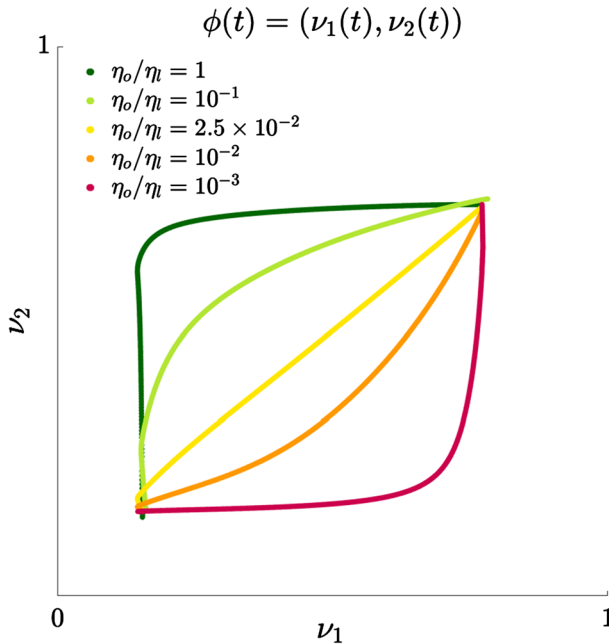


Fig. 8 Plots of the curve $\phi(t) = (\nu_1(t), \nu_2(t))$ for different values of the ratio between the selection gradient related to oxygen η_o and the selection gradient related to lactate η_l . The functions $\nu_1(t)$ and $\nu_2(t)$ defined via (3) model the levels of expression of the acidity-resistant gene and the hypoxia-resistant gene across the whole tissue region, respectively (Color figure online)

gene across the whole tissue region) and, for all values of η_o/η_l considered, ultimately converges to a point corresponding to a high expression level of both the acidity-resistant gene and the hypoxia-resistant gene. However, larger values of the ratio η_o/η_l lead the level of expression of the hypoxia-resistant gene $\nu_2(t)$ to increase faster than the level of expression of the acidity-resistant gene $\nu_1(t)$, while smaller values of η_o/η_l correlate with a faster increase of $\nu_1(t)$ and a slower increase of $\nu_2(t)$. Furthermore, for intermediate values of the ratio η_o/η_l we observe a simultaneous increase of the values of $\nu_1(t)$ and $\nu_2(t)$, whereas sufficiently large and sufficiently small values of η_o/η_l correlate with a decoupling between the increase of $\nu_1(t)$ and $\nu_2(t)$. In more detail, if the ratio η_o/η_l is sufficiently high, first $\nu_2(t)$ increases while $\nu_1(t)$ remains almost constant, and then, when $\nu_2(t)$ is sufficiently high, $\nu_1(t)$ starts increasing as well. On the other hand, in the case where η_o/η_l is sufficiently low, we have that $\nu_1(t)$ increases first and then $\nu_2(t)$ starts increasing as soon as $\nu_1(t)$ becomes sufficiently high.

These results communicate the biological notion that: the strength of the selective pressures exerted by oxygen and lactate on tumour cells, which are quantified by the values of the selection gradients η_o and η_l , may shape the emergence of hypoxic resistance and acidic resistance in tumours; the order in which such forms of resistance develop depends on the intensity of oxygen-driven selection in relation to the intensity of lactate-driven selection.

4 Conclusions and Research Perspectives

In this work, we have developed a mathematical modelling approach to investigate the influence of hypoxia and acidity on the evolutionary dynamics of cancer cells in vascularised tumours.

The results of numerical simulations of a calibrated version of the model based on real data recapitulate the eco-evolutionary spatial dynamics of tumour cells and their adaptation to hypoxic and acidic microenvironments. In particular, the results obtained indicate that tumour cells characterised by lower levels of expression of hypoxia- and acidity-resistant genes are to be expected to colonise well-oxygenated and mildly acidic regions of vascularised tissues, whereas cells expressing a more aggressive phenotype characterised by higher levels of resistance to hypoxia and acidity will ultimately populate tissue regions corresponding to hypoxic and acidic microenvironments. Such theoretical findings recapitulate histological data on ductal carcinoma *in situ*, showing that the levels at which the acidity-resistant gene LAMP2 and the hypoxia-resistant gene GLUT-1 are expressed by cancer cells increase moving from the walls to the centre of the milk duct (i.e. moving from more oxygenated and less acidic regions to regions that are less oxygenated and more acidic) (Damaghi et al. 2015; Gatenby et al. 2007).

Moreover, our theoretical findings reconcile the conclusions of Gatenby et al. (2007), suggesting that tumour cells acquire first resistance to hypoxia and then resistance to acidity, and the conclusions of Robertson-Tessi et al. (2015), supporting the idea that the two forms of resistance are acquired in reverse order, by showing that the order in which resistance to hypoxia and resistance to acidity arise depend on the ways in which oxygen and lactate act as environmental stressors in the evolutionary dynamics of tumour cells, which are known to vary between tissue types and between patients (Maley et al. 2017).

We conclude with a brief overview of possible research perspectives. Along the lines of Lorenzi et al. (2021), the modelling framework presented here could be extended to incorporate additional details of cell movement and mechanical interactions between cells (Ambrosi and Preziosi 2002; Astanin and Preziosi 2008; Byrne and Preziosi 2003), which would make it possible to investigate the interplay between phenotypic evolution of cancer cells and tumour growth. Alternative ways of modelling the effect of heritable, spontaneous phenotypic changes, for instance via integral terms (Barles et al. 2009; Busse et al. 2020; Calsina et al. 2013; Diekmann et al. 2005; Lorz et al. 2013), could also be considered, in order to capture finer details of the processes that drive phenotypic changes (Amadori et al. 2015, 2018; Carja and Plotkin 2017; Champagnat et al. 2006; Di Costanzo et al. 2018). Moreover, it would be relevant to include in the model the effects of stress-induced phenotypic changes caused by hypoxia and acidity, which might be taken into account by introducing a drift term in the balance equation for the local population density function of tumour cells, as similarly done in Celora et al. (2021), Chisholm et al. (2015), Lorenzi et al. (2015). In the vein of Alfaro and Veruete (2019), Lorenzi and Pouchol (2020), Michod et al. (2006), Nguyen et al. (2019), it would also be interesting to consider possible generalisations of the definition of the fitness function employed here, for instance by letting the selection gradients depend on the concentrations of the abiotic factors, which would

allow the concavity of the fitness function to vary across the tumour depending on the local environmental conditions, and by introducing multiple fitness peaks, in order to explore alternative ways in which the spatial and evolutionary dynamics of tumour cells, and their dynamical interactions with abiotic factors, may drive the emergence of intra-tumour phenotypic heterogeneity (Gerlinger et al. 2012).

Building on Ardaševa et al. (2020a), it would be interesting to generalise the model to study the effects of fluctuations in the inflow rate of oxygen and glucose and the outflow rate of lactate in the evolution of cancer cells. In fact, when in hypoxic conditions, cancer cells are known to produce and secrete proangiogenic factors which induce the formation of new blood vessels departing from existing ones. Such an angiogenic process results in the formation of a disordered tumour vasculature whereby the rates at which oxygen and glucose enter the tumour and the rate at which lactate is flushed out through intra-tumour blood vessels fluctuate over time, which impacts on the evolutionary dynamics of cancer cells (Dewhirst 2009; Kimura et al. 1996; Matsumoto et al. 2010; Michiels et al. 2016).

It would also be interesting to extend the model in order to investigate the role of phenotypic transitions triggered by hypoxia and acidity—such as the epithelial–mesenchymal transition induced by hypoxic environmental conditions (Misra and Pandey 2012; Tam et al. 2020; Zhang et al. 2015) and the acquisition of the metastatic phenotype promoted by acidic microenvironments (Damaghi et al. 2015; DeClerck and Elble 2010; Fais et al. 2014)—in the phenotypic adaptation of cancer cells and tumour growth.

Furthermore, since resistance to hypoxia is known to correlate with resistance to chemotherapy and radiotherapy (Cosse and Michiels 2008; DeClerck and Elble 2010; Lewin et al. 2018; Prokopiou et al. 2015; Teicher 1994), building on Chaplain et al. (2021); Lorenzi et al. (2018); Lorz et al. (2015), it would be relevant for anti-cancer therapy to address numerical optimal control for an extended version of the model that takes into account the effect of chemotherapy and/or radiotherapy (Almeida et al. 2019; Pouchol et al. 2018), which could inform the development of optimised cancer treatment protocols that exploit evolutionary and ecological principles (Acar et al. 2020; Gatenby et al. 2009; Korolev et al. 2014; Merlo et al. 2006).

Finally, it would certainly be interesting to extend the model presented here to two- and three-dimensional spatial domains. This would make it possible to explore the evolutionary dynamics of tumour cells in a broader range of biological and clinical scenarios and, in particular, it would allow to investigate how the level of tissue vascularisation and the distribution of blood vessels may affect the eco-evolutionary process leading to the emergence of resistance to hypoxia and acidity in vascularised tumours.

Funding Open access funding provided by Politecnico di Torino within the CRUI-CARE Agreement.

Declaration

Conflict of interest The authors declare that they have no conflict of interest.

Open Access This article is licensed under a Creative Commons Attribution 4.0 International License, which permits use, sharing, adaptation, distribution and reproduction in any medium or format, as long as you give appropriate credit to the original author(s) and the source, provide a link to the Creative Commons licence,

and indicate if changes were made. The images or other third party material in this article are included in the article’s Creative Commons licence, unless indicated otherwise in a credit line to the material. If material is not included in the article’s Creative Commons licence and your intended use is not permitted by statutory regulation or exceeds the permitted use, you will need to obtain permission directly from the copyright holder. To view a copy of this licence, visit <http://creativecommons.org/licenses/by/4.0/>.

A Steady-State Properties of the Model for the Dynamics of Tumour Cells and Robustness of the Results Obtained

Steady-State Properties of the model for the dynamics of tumour cells Using a time scale separation approach and a formal asymptotic method similar to those employed in Villa et al. (2021), one can formally show that when spontaneous phenotypic changes and undirected, random cell movement occur on slower time scales compared to cell division and death, as in the case of this work (cf. the parameter values listed in Table 1), and the fitness function $R(S_o, S_g, S_l, \rho, y_1, y_2)$ is a strictly concave function of $\mathbf{y} = (y_1, y_2)$ of the form considered here, i.e.

$$R(S_o, S_g, S_l, \rho, y_1, y_2) := p(S_o, S_g, S_l, y_1, y_2) - \kappa\rho \tag{22}$$

with

$$p(S_o, S_g, S_l, y_1, y_2) := \frac{\gamma_o S_o}{\alpha_o + S_o} (1 - \varphi_o(S_o)) + \frac{\gamma_g S_g}{\alpha_g + S_g} \varphi_o(S_o) - \eta_o (y_2 - \varphi_o(S_o))^2 - \eta_l (y_1 - \varphi_l(S_l))^2 \tag{23}$$

where $\varphi_o : \mathbb{R}^+ \rightarrow [0, 1]$ and $\varphi_l : \mathbb{R}^+ \rightarrow [0, 1]$, the steady-state distribution of tumour cells, $n^\infty(x, y_1, y_2)$, will be unimodal and such that the steady-state cell density,

$$\rho^\infty(x) = \int_0^1 \int_0^1 n^\infty(x, y_1, y_2) dy_1 dy_2,$$

the steady-state local mean level of expression of the acidity-resistant gene,

$$\mu_1^\infty(x) = \frac{1}{\rho^\infty(x)} \int_0^1 \int_0^1 y_1 n^\infty(x, y_1, y_2) dy_1 dy_2,$$

and the steady-state local mean level of expression of the hypoxia-resistant gene,

$$\mu_2^\infty(x) = \frac{1}{\rho^\infty(x)} \int_0^1 \int_0^1 y_2 n^\infty(x, y_1, y_2) dy_1 dy_2,$$

will satisfy the following system

$$\begin{cases} R\left(S_o^\infty(x), S_g^\infty(x), S_l^\infty(x), \rho^\infty(x), \mu_1^\infty(x), \mu_2^\infty(x)\right) = 0, \\ \frac{\partial R}{\partial y_1}\left(S_o^\infty(x), S_g^\infty(x), S_l^\infty(x), \rho^\infty(x), \mu_1^\infty(x), \mu_2^\infty(x)\right) = 0, \\ \frac{\partial R}{\partial y_2}\left(S_o^\infty(x), S_g^\infty(x), S_l^\infty(x), \rho^\infty(x), \mu_1^\infty(x), \mu_2^\infty(x)\right) = 0, \end{cases} \quad \forall x \in [0, L],$$

where $S_o^\infty(x)$, $S_g^\infty(x)$ and $S_l^\infty(x)$ are the steady-state concentrations of oxygen, glucose and lactate, respectively.

Substituting definitions (22) and (23) into the above system and solving for ρ^∞ , μ_1^∞ and μ_2^∞ yields

$$\rho^\infty(x) = \frac{1}{\kappa} \left(\frac{\gamma_o S_o^\infty(x)}{\alpha_o + S_o^\infty(x)} (1 - \varphi_o(S_o^\infty(x))) + \frac{\gamma_g S_g^\infty(x)}{\alpha_g + S_g^\infty(x)} \varphi_o(S_o^\infty(x)) \right) \quad (24)$$

and

$$\mu_1^\infty(x) = \varphi_l(S_l^\infty(x)), \quad \mu_2^\infty(x) = \varphi_o(S_o^\infty(x)). \quad (25)$$

These formal results are confirmed both by the plots in Fig. 6c–e, which show that, at every position $x \in [0, L]$, the local phenotypic distribution of tumour cells at the end of numerical simulations $n(T, x, \mathbf{y})$ is unimodal, and by the plots in Fig. 9, which demonstrate that, defining $S_o^\infty(x)$, $S_g^\infty(x)$ and $S_l^\infty(x)$ as $S_o(T, x)$, $S_g(T, x)$ and $S_l(T, x)$ displayed in Fig. 4, respectively, and using the same parameter values as those used to obtain the numerical results of Figs. 4 and 6, there is an excellent quantitative match between: $\rho^\infty(x)$ defined via (24) and $\rho(T, x)$ displayed in Fig. 4; $\mu_1^\infty(x)$ defined via (25) and $\mu_1(T, x)$ displayed in Fig. 6; $\mu_2^\infty(x)$ defined via (25) and $\mu_2(T, x)$ displayed in Fig. 6.

Robustness of the Results Obtained From the form of the steady-state cell density ρ^∞ given by (24), the form of the steady-state local mean level of expression of the acidity-resistant gene μ_1^∞ given by (25), and the form of the steady-state local mean level of expression of the hypoxia-resistant gene μ_2^∞ given by (25), one can see that the qualitative properties of the results presented in Sects. 3.2 and 3.3—i.e. the fact that:

- (i) the plateau value of the cell density ρ decreases with the distance from the blood vessel;
- (ii) the local mean level of expression of the acidity-resistant gene μ_1 at equilibrium is the minimal one in mildly acidic regions, the maximal one in highly acidic conditions and increases with the lactate concentration in moderately acidic environments;

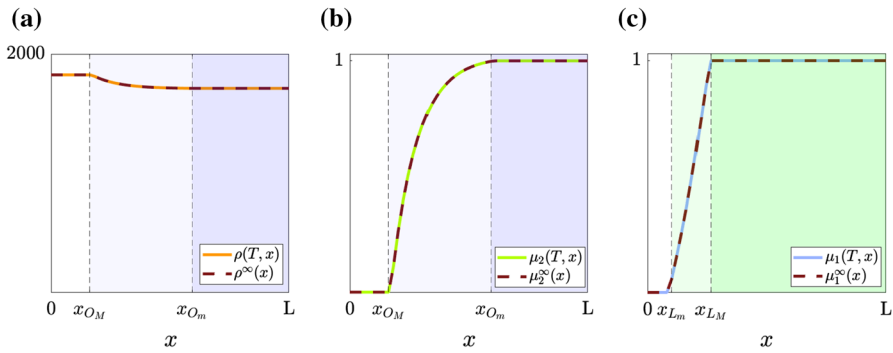


Fig. 9 **a** Comparison between $\rho^\infty(x)$ defined via (24) (dashed line) and $\rho(T, x)$ displayed in Fig. 4 (solid line). **b** Comparison between $\mu_2^\infty(x)$ defined via (25) (dashed line) and $\mu_2(T, x)$ displayed in Fig. 6 (solid line). **c** Comparison between $\mu_1^\infty(x)$ defined via (25) (dashed line) and $\mu_1(T, x)$ displayed in Fig. 6 (solid line). Here, $\rho^\infty(x)$, $\mu_1^\infty(x)$ and $\mu_2^\infty(x)$ are computed defining $S_o^\infty(x)$, $S_g^\infty(x)$ and $S_l^\infty(x)$ as $S_o(T, x)$, $S_g(T, x)$ and $S_l(T, x)$ displayed in Fig. 4, and using the same parameter values as those used to obtain the numerical results of Figs. 4 and 6 (cf. Table 1) (Color figure online)

- (iii) the local mean level of expression of the hypoxia-resistant gene μ_2 at equilibrium is the minimal one in normoxic conditions, the maximal one in hypoxic conditions and increases with the oxygen concentration in moderately oxygenated environments
 - remain intact under a broad range of parameter values.

References

Acar A, Nichol D, Fernandez-Mateos J, Cresswell GD, Barozzi I, Hong SP, Trahearn N, Spiteri I, Stubbs M, Burke R et al (2020) Exploiting evolutionary steering to induce collateral drug sensitivity in cancer. *Nat Commun* 11(1):1–14

Ambrosi D, Preziosi L (2002) On the closure of mass balance models for tumor growth. *Math Models Methods Appl Sci* 12(5):737–754

Alfaro M, Veruete M (2019) Evolutionary branching via replicator-mutator equations. *J Dyn Differ Equ* 31(4):2029–2052

Almeida L, Bagnerini P, Fabrini G, Hughes BD, Lorenzi T (2019) Evolution of cancer cell populations under cytotoxic therapy and treatment optimisation: insight from a phenotype-structured model. *ESAIM. Math Model Numer Anal* 53(4):1157–1190

Amadori AL, Calzolari A, Natalini R, Torti B (2015) Rare mutations in evolutionary dynamics. *J Differ Equ* 259(11):6191–6214

Amadori AL, Natalini R, Palmigiani D (2018) A rare mutation model in a spatial heterogeneous environment. *Ecol Complex* 34:188–197

Anderson ARA, Quaranta V (2008) Integrative mathematical oncology. *Nat Rev Cancer* 8(3):227–234

Anderson ARA, Weaver AM, Cummings PT, Quaranta V (2006) Tumor morphology and phenotypic evolution driven by selective pressure from the microenvironment. *Cell* 127(5):905–915

Anderson ARA, Rejniak KA, Gerlee P, Quaranta V (2009) Microenvironment driven invasion: a multiscale multimodel investigation. *J Math Biol* 58(4–5):579

Ardaševa A, Gatenby RA, Anderson ARA, Byrne HM, Maini PK, Lorenzi T (2020a) A mathematical dissection of the adaptation of cell populations to fluctuating oxygen levels. *Bull Math Biol* 82(6):81

- Ardaševa A, Gatenby RA, Anderson ARA, Byrne HM, Maini PK, Lorenzi T (2020b) Evolutionary dynamics of competing phenotype-structured populations in periodically fluctuating environments. *J Math Biol* 80(3):775–807
- Astanin S, Preziosi L (2008) Multiphase models of tumour growth. In: Bellomo N, de Angelis E (eds) *Selected topics in cancer modeling*. Birkhäuser, Boston, pp 1–31
- Astanin S, Preziosi L (2009) Mathematical modelling of the Warburg effect in tumour cords. *J Theor Biol* 258(4):578–590
- Barles G, Mirrahimi S, Perthame B et al (2009) Concentration in Lotka-Volterra parabolic or integral equations: a general convergence result. *Methods Appl Anal* 16(3):321–340
- Berestycki H, Hamel F (2012) Generalized transition waves and their properties. *Commun Pure Appl Math* 65(5):592–648
- Berestycki H, Nadin G (2020) Asymptotic spreading for general heterogeneous Fisher-KPP type equations. *Memoirs American Mathematical Society*, In press
- Bouin E, Calvez V, Meunier N, Mirrahimi S, Perthame B, Raoul G, Voituriez R (2012) Invasion fronts with variable motility: phenotype selection, spatial sorting and wave acceleration. *C R Math* 350(15–16):761–766
- Busse J-E, Cuadrado S, Marciniak-Czochra A (2020) Local asymptotic stability of a system of integro-differential equations describing clonal evolution of a self-renewing cell population under mutation. *arXiv preprint arXiv:2004.05353*
- Byrne HM (2010) Dissecting cancer through mathematics: from the cell to the animal model. *Nat Rev Cancer* 10(3):221–230
- Byrne HM, Preziosi L (2003) Modelling solid tumour growth using the theory of mixtures. *Math Med Biol J IMA* 20(4):341–366
- Calsina À, Cuadrado S, Desvillettes L, Raoul G (2013) Asymptotics of steady states of a selection-mutation equation for small mutation rate. *Proc Sect A Math R Soc Edinb* 143(6):1123
- Carja O, Plotkin JB (2017) The evolutionary advantage of heritable phenotypic heterogeneity. *Sci Rep* 7(1):1–12
- Casciari JJ, Sotirchos SV, Sutherland RM (1992) Variations in tumor cell growth rates and metabolism with oxygen concentration, glucose concentration, and extracellular pH. *J Cell Physiol* 151(2):386–394
- Celora GL, Byrne HM, Zois C, Kevrekidis PG (2021) Phenotypic variation modulates the growth dynamics and response to radiotherapy of solid tumours under normoxia and hypoxia. *arXiv preprint arXiv:2101.05563*
- Champagnat N, Ferrière R, Méléard S (2006) Unifying evolutionary dynamics: from individual stochastic processes to macroscopic models. *Theor Popul Biol* 69(3):297–321
- Chaplain MAJ (2020) Multiscale modelling of cancer: micro-, meso- and macro-scales of growth and spread. In: Bizzarri M (ed) *Approaching complex diseases*. Springer, Berlin, pp 149–168
- Chaplain MAJ, Lorenzi T, Villa C (2021) Evolutionary dynamics in vascularised tumours under chemotherapy. *Vietnam J Math* 49:143–167
- Chisholm RH, Lorenzi T (2016) Cell population heterogeneity and evolution towards drug resistance in cancer: biological and mathematical assessment, theoretical treatment optimisation. *Biochim Biophys Acta (BBA) Genet Subj* 1860(11):2627–2645
- Chisholm RHC, Lorenzi T, Lorz A, Larsen AK, de Almeida LN, Escargueil A, Clairambault J (2015) Emergence of drug tolerance in cancer cell populations: an evolutionary outcome of selection, non-genetic instability and stress-induced adaptation. *Cancer Res* 75(6):930–939
- Chisholm RH, Lorenzi T, Desvillettes L, Hughes BD (2016) Evolutionary dynamics of phenotype-structured populations: from individual-level mechanisms to population-level consequences. *Zeitschrift für angewandte Mathematik und Physik* 67(100):1–34
- Cosse J-P, Michiels C (2008) Tumour hypoxia affects the responsiveness of cancer cells to chemotherapy and promotes cancer progression. *Anti-Cancer Agents Med Chem* 8(7):790–797
- Damaghi M, Tafreshi NK, Lloyd MC, Sprung RW, Estrella VC, Wojtkowiak JW, Morse DL, Koomen JM, Bui MM, Gatenby RA, Gillies RJ (2015) Chronic acidosis in the tumour microenvironment selects for overexpression of LAMP2 in the plasma membrane. *Nat Commun* 6:8752
- DeClerck K, Elble RC (2010) The role of hypoxia and acidosis in promoting metastasis and resistance to chemotherapy. *Front Biosci* 15:213–225
- Dewhirst MW (2009) Relationships between cycling hypoxia, HIF-1, angiogenesis and oxidative stress. *Radiat Res* 172(6):653–665

- Di Costanzo E, Giacomello A, Messina E, Natalini R, Pontrelli G, Rossi F, Smits R, Twarogowska M (2018) A discrete in continuous mathematical model of cardiac progenitor cells formation and growth as spheroid clusters (Cardiospheres). *Math Med Biol J IMA* 35(1):121–144
- Diekmann O, Jabin P-E, Mischler S, Perthame B (2005) The dynamics of adaptation: an illuminating example and a Hamilton-Jacobi approach. *Theor Popul Biol* 67(4):257–271
- Doerfler W, Böhm P (2006) DNA methylation: development, genetic disease and cancer. Springer, Berlin, p 310
- Duesberg P, Stindl R, Hehlmann R (2000) Explaining the high mutation rates of cancer cells to drug and multidrug resistance by chromosome reassortments that are catalyzed by aneuploidy. *Proc Natl Acad Sci* 97(26):14295–14300
- Eastman B, Wodarz D, Kohandel M (2020) The effects of phenotypic plasticity on the fixation probability of mutant cancer stem cells. *J Theor Biol* 503:110384
- Fais S, Venturi G, Gatenby B (2014) Microenvironmental acidosis in carcinogenesis and metastases: new strategies in prevention and therapy. *Cancer Metastasis Rev* 33(4):1095–1108
- Iglesias SF, Mirrahimi S (2018) Long time evolutionary dynamics of phenotypically structured populations in time-periodic environments. *SIAM J Math Anal* 50(5):5537–5568
- Gallaher J, Anderson ARA (2016) Evolution of intratumoral phenotypic heterogeneity: the role of trait inheritance. *Interface Focus* 3(4):20130016
- Gallaher JA, Brown J, Anderson ARA (2019) The impact of proliferation-migration tradeoffs on phenotypic evolution in cancer. *Sci Rep* 9:2425
- Gatenby RA, Gawlinski ET (1996) A reaction-diffusion model of cancer invasion. *Cancer Res* 56(24):5745–5753
- Gatenby RA, Smallbone K, Maini PK, Rose F, Averill JG, Nagle RB, Worrall LJ, Gillies RJ (2007) Cellular adaptations to hypoxia and acidosis during somatic evolution of breast cancer. *Br J Cancer* 97(5):646–653
- Gatenby RA, Silva AS, Gillies RJ, Frieden BR (2009) Adaptive therapy. *Cancer Res* 69(11):4894–4903
- Gay L, Baker A-M, Graham TA (2016) Tumour cell heterogeneity, Faculty of 1000 Ltd, 5
- Genieys S, Volpert V, Auger P (2006) Adaptive dynamics: modelling Darwin's divergence principle. *C R Biol* 329(11):876–879
- Gerlinger M, Rowan AJ, Horswell S, Larkin S, Endesfelder D, Gronroos E, Martinez P, Matthews N, Stewart A, Tarpey P et al (2012) Intratumor heterogeneity and branched evolution revealed by multiregion sequencing. *New Engl J Med* 366:883–892
- Gillies RJ, Verduzco D, Gatenby RA (2012) Evolutionary dynamics of carcinogenesis and why targeted therapy does not work. *Nat Rev Cancer* 12(7):487–493
- Hamis SJ, Powathil GG (2020) Can we crack cancer? In: Matthäus F, Matthäus S, Harris S, Hillen T (eds) *The art of theoretical biology*. Springer, Berlin, pp 50–51
- Hatzikirou H, Basanta D, Simon M, Schaller K, Deutsch A (2012) 'Go or grow': the key to the emergence of invasion in tumour progression? *Math Med Biol J IMA* 29(1):49–65
- Hockel M, Vaupel P (2001) Tumor hypoxia: definitions and current clinical, biologic, and molecular aspects. *J Natl Cancer Inst* 93(4):266–276
- Ibrahim-Hashim A, Robertson-Tessi M, Enriquez-Navas PM, Damaghi M, Balagurunathan Y, Wojtkowiak JW, Russell S, Yoonseok K, Lloyd MC, Bui MM et al (2017) Defining cancer subpopulations by adaptive strategies rather than molecular properties provides novel insights into intratumoral evolution. *Cancer Res* 77(9):2242–2254
- Kim J-W, Dang CV (2006) Cancer's molecular sweet tooth and the Warburg effect. *Cancer Res* 66(18):8927–8930
- Kim Y, Kang H, Powathil G, Kim H, Trucu D, Lee W, Lawler SE, Chaplain MAJ (2018) Role of extracellular matrix and microenvironment in regulation of tumor growth and LAR-mediated invasion in glioblastoma. *PLoS ONE* 13(10):e0204865
- Kimura H, Braun RD, Ong ET, Hsu R, Secomb TW, Papahadjopoulos D, Hong K, Dewhirst MW (1996) Fluctuations in red cell flux in tumor microvessels can lead to transient hypoxia and reoxygenation in tumor parenchyma. *Cancer Res* 56(23):5522–5528
- Korolev KS, Xavier JB, Gore J (2014) Turning ecology and evolution against cancer. *Nat Rev Cancer* 14(5):371–380
- LeVeque RJ (2007) Finite difference methods for ordinary and partial differential equations: steady-state and time-dependent problems. Society for Industrial and Applied Mathematics (SIAM), Philadelphia

- Lewin TD, Maini PK, Moros EG, Enderling H, Byrne HM (2018) The evolution of tumour composition during fractionated radiotherapy: implications for outcome. *Bull Math Biol* 80(5):1207–1235
- Lloyd MC, Cunningham JJ, Bui MM, Gillies RJ, Brown JS, Joel S, Gatenby RA (2016) Darwinian dynamics of intratumoral heterogeneity: not solely random mutations but also variable environmental selection forces. *Cancer Res* 76(11):3136–3144
- Loeb LA (2001) A mutator phenotype in cancer. *Cancer Res* 61(8):3230–3239
- Lorenzi T, Pouchol C (2020) Asymptotic analysis of selection-mutation models in the presence of multiple fitness peaks. *Nonlinearity* 33(11):5791
- Lorenzi T, Chisholm RH, Desvillettes L, Hughes BD (2015) Dissecting the dynamics of epigenetic changes in phenotype-structured populations exposed to fluctuating environments. *J Theor Biol* 386:166–176
- Lorenzi T, Chisholm RH, Clairambault J (2016) Tracking the evolution of cancer cell populations through the mathematical lens of phenotype-structured equations. *Biol Direct* 11(1):43
- Lorenzi T, Venkataraman C, Lorz A, Chaplain MAJ (2018) The role of spatial variations of abiotic factors in mediating intratumour phenotypic heterogeneity. *J Theor Biol* 451(14):101–110
- Lorenzi T, Perthame B, Ruan X (2021) Invasion fronts and adaptive dynamics in a model for the growth of cell populations with heterogeneous mobility. *Eur J Appl Math*, in press
- Lorz A, Lorenzi T, Hochberg ME, Clairambault J, Perthame B (2013) Populational adaptive evolution, chemotherapeutic resistance and multiple anti-cancer therapies. *ESAIM. Math Model Numer Anal* 47(2):377–399
- Lorz A, Lorenzi T, Clairambault J, Escargueil A, Perthame B (2015) Modeling the effects of space structure and combination therapies on phenotypic heterogeneity and drug resistance in solid tumors. *Bull Math Biol* 77(1):1–22
- Maley CC, Aktipis A, Graham TA, Sottoriva A, Boddy AM, Janiszewska M, Silva AS, Gerlinger M, Yuan Y, Pienta KJ et al (2017) Classifying the evolutionary and ecological features of neoplasms. *Nat Rev Cancer* 17(10):605–619
- Martinez-Outschoorn UE, Peiris-Pagés M, Pestell RG, Sotgia F, Lisanti MP (2016) Cancer metabolism: a therapeutic perspective. *Nat Rev Clin Oncol* 14(1):11–31
- Marusyk A, Almendro V, Polyak K (2012) Intra-tumour heterogeneity: a looking glass for cancer? *Nature Rev Cancer* 12(5):323–334
- Matsumoto S, Yasui H, Mitchell JB, Krishna MC (2010) Imaging cycling tumor hypoxia. *Cancer Res* 70(24):10019–10023
- Merlo LMF, Pepper JW, Reid BJ, Maley CC (2006) Cancer as an evolutionary and ecological process. *Nat Rev Cancer* 6(12):924–935
- Michiels C, Tellier C, Feron O (2016) Cycling hypoxia: a key feature of the tumor microenvironment. *Biochim Biophys Acta (BBA) Rev Cancer* 1866(1):76–86
- Michod RE, Viossat Y, Solari CA, Hurand M, Nedelcu AM (2006) Life-history evolution and the origin of multicellularity. *J Theor Biol* 239(2):257–272
- Michor F, Polyak K (2010) The origins and implications of intratumour heterogeneity. *Cancer Prev Res* 3(11):1361–1364
- Mirrahimi S, Gandon S (2020) Evolution of specialization in heterogeneous environments: equilibrium between selection, mutation and migration. *Genetics* 214(2):479–491
- Misra A, Pandey C, Sze SK, Thanabalu T (2012) Hypoxia activated EGFR signaling induces epithelial to mesenchymal transition (EMT). *PLoS ONE* 7(11):e49766
- Molavian HR, Kohandel M, Milosevic M, Sivaloganathan S (2009) Fingerprint of cell metabolism in the experimentally observed interstitial pH and pO₂ in solid tumors. *Cancer Res* 69(23):9141–9147
- Nguyen TN, Clairambault J, Jaffredo T, Perthame B, Salort D (2019) Adaptive dynamics of hematopoietic stem cells and their supporting stroma: a model and mathematical analysis. *Math Biosci Eng* 16(5):4818–4845
- Perthame B, Génieys S (2007) Concentration in the nonlocal Fisher equation: the Hamilton-Jacobi limit. *Math Model Nat Phenom* 2(4):135–151
- Poleszczuk J, Hahnfeldt P, Enderling H (2015) Evolution and phenotypic selection of cancer stem cells. *PLoS Comput Biol* 11(3):e1004025
- Pouchol C, Clairambault J, Lorz A, Trélat E (2018) Asymptotic analysis and optimal control of an integro-differential system modelling healthy and cancer cells exposed to chemotherapy. *Journal de Mathématiques Pures et Appliquées* 116:268–308

- Prokopiou S, Moros EG, Poleszczuk J, Caudell J, Torres-Roca JF, Latifi K, Lee JK, Myerson R, Harrison LB, Enderling H (2015) A proliferation saturation index to predict radiation response and personalize radiotherapy fractionation. *Radiat Oncol* 10(1):1–8
- Robertson-Tessi M, Gillies RJ, Gatenby RA, Anderson ARA (2015) Impact of metabolic heterogeneity on tumor growth, invasion, and treatment outcomes. *Cancer Res* 75(8):1567–1579
- Strobl MAR, Krause AL, Damaghi M, Gillies RJ, Anderson ARA, Maini PK (2020) Mix and match: phenotypic coexistence as a key facilitator of cancer invasion. *Bull Math Biol* 82(1):1–26
- Tam SY, Wu VWC, Law HKW (2020) Hypoxia-induced epithelial-mesenchymal transition in cancers: HIF-1 α and Beyond. *Front Oncol* 10:486
- Tang X, Lucas JE, Chen JL-Y, LaMonte G, Wu J, Wang MC, Koumenis C, Chi J-T (2012) Functional interaction between responses to lactic acidosis and hypoxia regulates genomic transcriptional outputs. *Cancer Res* 72(2):491–502
- Teicher BA (1994) Hypoxia and drug resistance. *Cancer Metastasis Rev* 13(2):139–168
- Vander Linden C, Corbet C (2020) Reconciling environment-mediated metabolic heterogeneity with the oncogene-driven cancer paradigm in precision oncology. *Semin Cell Dev Biol* 98:202–210
- Vaupel P, Thews O, Hoeckel M (2001) Treatment resistance of solid tumors: role of hypoxia and anemia. *Med Oncol* 18:243
- Villa C, Chaplain MA, Lorenzi T (2021) Modeling the emergence of phenotypic heterogeneity in vascularized tumors. *SIAM J Appl Math* 81(2):434–453
- Zhang W, Shi X, Peng Y, Wu M, Zhang P, Xie R, Wu Y, Yan Q, Wang SLJ (2015) HIF-1 α promotes epithelial-mesenchymal transition and metastasis through direct regulation of ZEB1 in colorectal cancer. *PLoS ONE* 10(6):e0129603

Publisher's Note Springer Nature remains neutral with regard to jurisdictional claims in published maps and institutional affiliations.